[AMERICAN JOURNAL OF SCIENCE, VOL. 295, NOVEMBER, 1995, P. 1156–1176]

GENESIS OF AGATES IN FLOOD BASALTS: TWISTING OF CHALCEDONY FIBERS AND TRACE-ELEMENT GEOCHEMISTRY

ENRIQUE MERINO,* YIFENG WANG,*
and ÉTIENNE DELOULE**

ABSTRACT. **Chalcedony layers in agates from the Paraná flood basalt contain alternatively high and low trace contents of Al, Fe, K, and Na, as measured with an ion-probe. They also contain Ni and Mn but no significant Li, Mg, or Ca. These oscillatory profiles confirm oscillations predicted by a self-organizational crystallization model (developed earlier) based on the joint operation of cation-enhanced quartz growth, which produces the banding, and morphologically unstable crystallization fronts, which generates the fibrous texture.**

Length-fast fibers that grow through strong decreasing trace-element gradients are forced to incorporate a higher content of the trace elements (substituting for Si) along their peripheries than along their centers. Since these trace ions (Al^{3+} and Fe^{3+}) are larger in size than Si^{4+}, the fibers have to grow twisted to accommodate the additional peripheric trace-element content. The twist period of a fiber, calculated such that the twisting produces just enough stretching to contain the peripheric trace element content, comes out proportional to the fiber radius and to the minus one-half power of the difference in cube roots of the trace-element contents along the periphery and along the center of the fiber. The ion-probe analyses also confirm this geometric constraint of the solid-solution twisting mechanism proposed here.

When plotted on an Al versus (Na+K+2Ni+2Fe) diagram (a diagram of substitutional versus interstitial cations), the ion-probe analyses of the agate oscillate along a unit-slope line and shift steadily toward the southeast of the diagram, a pattern consistent with the progressive oxidation of ferrous to ferric iron. This oxidation (by H_2O) is inevitably driven by the increase in both Fe^{2+} and H_2O concentrations produced by the very growth of the quartz layers. The Fe^{3+} so generated increasingly substitutes for silicon in quartz, makes the latest, drusy quartz purple, and causes occasional growth of goethite needles along with the latest quartz. The same oxidation also increases alkalinity and thus promotes zeolite growth, which accounts for the well-known association of zeolites with agates.

INTRODUCTION

Agates from flood basalts routinely display associated repetitive textures and trace-element-compositions. From its rim inward, an agate typically consists of a concentrically banded region, a coarse crystalline layer, and a central void. The banded region itself consists of layers made of fine-crystalline and untwisted quartz fibers that *alternate* with layers made of even finer and *twisted* fibers. The twisting can be seen easily

* Department of Geological Sciences, Indiana University, Bloomington, Indiana 47405. (Yifeng Wang's present address: Sandia National Laboratories, Department 6748, P.O. Box 5800, Albuquerque, New Mexico 87185.)

** Centre de Recherches Pétrologiques et Géochimiques, UPR A9046, CNRS, B.P. 20, 54501 Vandoeuvre-lès-Nancy, France.

under a microscope by the changing birefringence along any one fiber. All the fibers are length-fast—see Michel-Lévy and Munier Chalmas (1892), Frondel (1978), Merino (1984), and Wang and Merino (1990), and references therein for details.

We have proposed (Wang and Merino, 1990, 1995) a self-organizational reaction-transport model that predicts the observed inward sequence of textures, fibrous texture, associated alternations in fiber size, state of twisting and trace-element content, optical orientation of the fibers, and still other morphological, mineralogical, and optical properties of agates. The model, summarized in the next section, is based on the simultaneous operation of an autocatalytic-like growth reaction (which produces the banding) and a morphological instability of the reaction front (which generates the fibrous texture).

Our purpose here is to report the results of band-by-band ion- and electron-microprobe analyses of trace elements in two agates and to test in detail the hypothesis that quartz fibers that are forced to substitute Al^{3+} (or other trace elements) for Si^{4+} along their periphery must grow twisted to make room for the larger cations. We give a geometric calculation of the twist period that would be produced by that substitution. The analyses confirm the oscillatory trace-element profiles predicted in our previous work. When inserted into the geometric framework of the twisting model, the trace-element analyses yield predictions of twist period that match the observed twist periods as well as their oscillations. In light of the microanalyses we discuss the striking geochemistry of chalcedony and amethyst in agates.

CRYSTALLIZATION MODEL SUMMARY AND GENESIS OF FIBER TWISTING

As hypothesized in Macpherson (1989), Gonthier and others (1988), Wang and Merino (1990, 1995), and other references therein, agates probably crystallize not from aqueous solutions but from lumps of polymeric silica containing trace elements and water. Our model of agate crystallization (Wang and Merino, 1990, 1995; Merino, Wang, and Deloule, 1994) is based on the ideas that cations at the crystallization front can accelerate quartz growth and that the fibrous texture characteristic of agates is produced by a morphological instability of the crystallization front. The model predicts that the silica lumps can crystallize in an oscillatory fashion, acquiring repetitive features through self-organization. (Self-organization refers to the spontaneous generation of patterns through the system's own dynamics; see Nicolis and Prigogine, 1977, 1989.) Quartz bands are predicted to incorporate *oscillating* amounts of trace elements, some substituting for Si^{4+} and some balancing the charge loss incurred by the substitution.

At the same time morphologically unstable crystallization fronts cause *fibers* to form. Small random bumps on an unstable front tend to grow longer and to produce more bumps next to them (Wang and Merino, 1995). Competition among neighboring bumps, which become

fibers, determines the thickness of the fibers. The length of the fibers is determined by surface energy and by the concentration gradients of silica and trace elements just ahead of the crystallization front. Because the concentration gradients themselves oscillate, the fiber size is predicted to change periodically, as observed in agates. The model predicts that finer quartz fibers should contain higher trace element contents than less fine ones (Wang and Merino, 1995).

Because of the roughly conical shape of the bumps, fibers are likely to grow by addition of *conical* sleeves (as in Langer's fig. 12, 1980).[1] If so, the sleeves, as they grow, must cut across decreasing Al and/or Fe concentrations (fig. 1). Their bases are thus forced (by the mass-action law) to incorporate more Al (and/or Fe) than their apices, and the ensemble of successive such sleeves yields a fiber with higher trace-element content along its periphery than along its center (fig. 1). The Al and/or Fe, upon substitution for Si, because their radii are larger than Si's, should deform the structure of quartz, just as $Al^{(IV)}$ deforms the structure of halloysite (Merino, Harvey, and Murray, 1989). Since the dilatation is greater (because of the higher trace-element content) in the outer unit cells of a fiber than in those along its axis, and since the dilatation must occur, not in the plane of the cross section (because all peripheric cells have the same space problem), but along the length of the fiber, the fiber has no geometric freedom *but to become twisted* to make room for the higher trace-element content in its outer layers. Keith and Padden (1961) proposed a related origin for the twisting of organic polymer fibers. We calculate below the degree of twisting hypothetically produced by substitution of trace elements for Si in agate quartz fibers and then summarize all predictions of the model.

GEOMETRY OF QUARTZ-FIBER TWISTING

The following calculation is based on that given in Wang and Merino (1990, p. 1636), but it explicitly takes account of the *difference* in trace-element content between the center and the periphery of a fiber and corrects errors made in our earlier paper. In the equations below we refer to substitution of Al for Si, but Fe^{3+} (see below) and other cations also may substitute for Si in agates, and the calculation also applies to these latter cations.

For a quartz fiber of radius R (fig. 2) having c_c ppm Al along its center and c_p ppm Al along its periphery, with $c_p > c_c$,

$$(\ell')^2 = \ell^2 + 4\pi^2 R^2. \tag{1}$$

The lengths ℓ (which is the twist period, or fiber length over which the twist is 2π) and ℓ' (which is the stretched length at the periphery of the

[1] Fibers are built probably with c-parallel silica-polymer-chain molecules from the initial medium that arrange themselves parallel to each other and flat on the fiber's growing surface (Folk and Pittman, 1971). This is what makes the fibers systematically length-fast.

fiber) are

$$\ell = n_{SiO}L_{SiO} + n_{AlO}L_{AlO}$$
$$\ell' = n'_{SiO}L_{SiO} + n_{AlO}L_{AlO}$$
$$n'_{SiO} + n'_{AlO} = n_{SiO} + n_{AlO} \qquad (2)$$

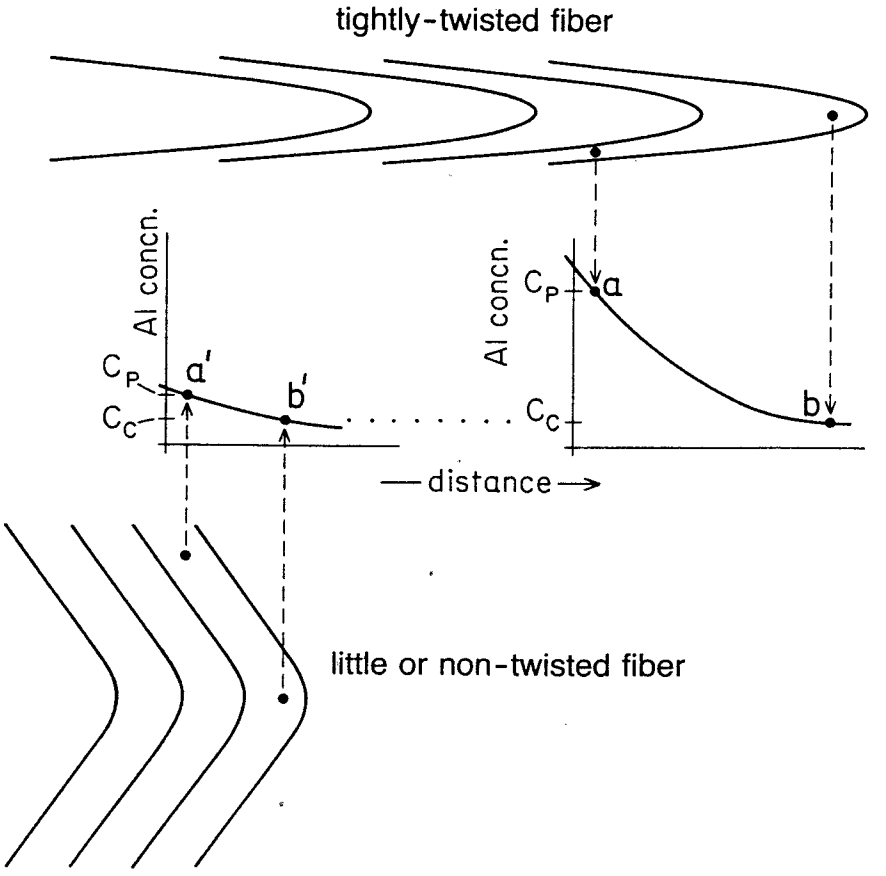

Fig. 1. Each quartz fiber grows by accretion of conical sleeves. As each sleeve pierces through a decreasing trace-element profile, its rim is forced to incorporate (in substitution for Si) a higher trace-element content than its tip is; the substituting ions are Al^{3+} and/or Fe^{3+}. The radial cation gradient thus generated in each fiber forces it to grow twisted to make room for its greater peripheric trace-element content. When the front is morphologically very unstable (top) the fiber becomes very thin and long, and its trace-element-content difference between center and periphery is relatively large, and its twist period consequently very small (eq 7); this corresponds to a point at about middle left in figure 3. When the morphological instability becomes less pronounced, fibers become thicker and shorter (bottom), their $(c_p - c_c)$ very low, and their twist period enormous (yielding practically untwisted fibers), corresponding to a point toward the bottom left of figure 3.

The lengths L are bond lengths, and the primed and non-primed n's are the numbers of subscripted bonds in the lengths ℓ' and ℓ, respectively, Using

$$\frac{n_{AlO}}{n_{SiO}} = ac_c^{1/3}; \qquad \frac{n'_{AlO}}{n'_{SiO}} = ac_p^{1/3} \tag{3}$$

and eqs (2), one obtains

$$\frac{\ell}{\ell'} = \frac{(1 + ac_p^{1/3})(1 + iac_c^{1/3})}{(1 + ac_c^{1/3})(1 + iac_p^{1/3})}, \tag{4}$$

where

$$a = 0.01\left(\frac{W_{SiO_2}}{W_{Al}}\right)^{1/3}, \qquad i = L_{AlO}/L_{SiO}. \tag{5}$$

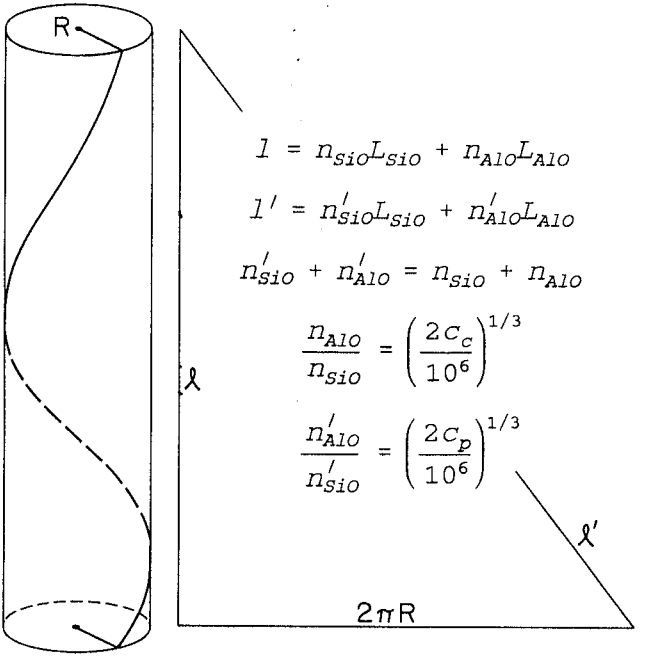

Fig. 2. Calculation of the twist period, ℓ, of a chalcedony fiber, correcting the calculation in figure 9 of Wang and Merino (1990). The contents of the trace-ion substituting for Si along the center and periphery of the cylindrical fiber are c_c and c_p ppm's respectively. Because the trace-O bond is always longer than a SiO bond, the periphery must lengthen (for which the fiber must twist) in order to make enough room to house the additional peripheric trace cations.

The W's are gram formula weights. Eqs (3) correct an error in Wang and Merino (1990, p. 1636), where we took $n_{AlO}/n_{SiO} = 2c/10^6$. Through the cube roots, eqs (3) now take account of the fact that concentrations refer to a mass (or a volume) of quartz, whereas the ratios of bond numbers in eq (3) are along a linear dimension.

We solve for ℓ' from (4), replace into (1), and solve for the twist period ℓ. Because $a = (W_{SiO2}/10^6\ W_{Al})^{1/3} = 0.01305$ and $i = 1.07$ (Wedepohl, 1970 p. 14A3; Geisinger, Gibbs, and Navrotsky, 1985), we neglect terms in a^2 and higher powers. (i differs little from 1.07 for trace elements other than Al.) The result is

$$\ell \simeq 2\pi R \left(\frac{1 + 2a(ic_p^{1/3} + c_c^{1/3})}{2a(i-1)(c_p^{1/3} - c_c^{1/3})} \right)^{1/2}, \tag{6}$$

or, using values for a and i,

$$\ell \simeq 147R \left(\frac{1 + 0.026\ (c_p^{1/3} + c_c^{1/3})}{c_p^{1/3} - c_c^{1/3}} \right)^{1/2}. \tag{7}$$

The AlO and SiO bonds are assumed to be roughly parallel to the fiber axis, which is not true, so the right side of eq (7) should be multiplied by the cosine of the angle between axis and bond. This angle appears to be, for alternate bonds, roughly 20° and 45° on figure 165 of Deer, Howie, and Zussman (1992, p. 459).

According to the genesis of fibrous agates textures hypothesized in Wang and Merino (1995), higher trace-element concentrations at the crystallization front make the front morphologically more unstable (that is, fibers become finer and more pointed, see fig. 1) and also cause the concentration gradients of trace elements ahead of the front to be more negative, inevitably resulting in a larger Al content difference between a fiber's center and its periphery. During oscillatory crystallization of agate layers, a point representing the system moves repeatedly up and down roughly along a north-northeasterly direction on figure 3 (that is, fibers become more and less twisted). Simultaneously, because of the spontaneous oscillations in the morphological instability of the growth front (Wang and Merino, 1995, fig. 7), the fibers become thin toward the top of figure 3 and thick toward the bottom. This implies that very thin, tightly twisted fibers should contain more (average) Al than coarser, untwisted fibers.

ELECTRON PROBE ANALYSES

Analyses for Al, K, Na, Ti, and Fe were made at 50 points on 5 untwisted-fiber and 5 intervening twisted-fiber agate bands in sample 8001 from Rio Grande do Sul, Brazil, with the 4-spectrometer Camebax electron microprobe of the Service Commun Microsonde at the University of Montpellier II. Photomicrographs of this agate are in Wang and

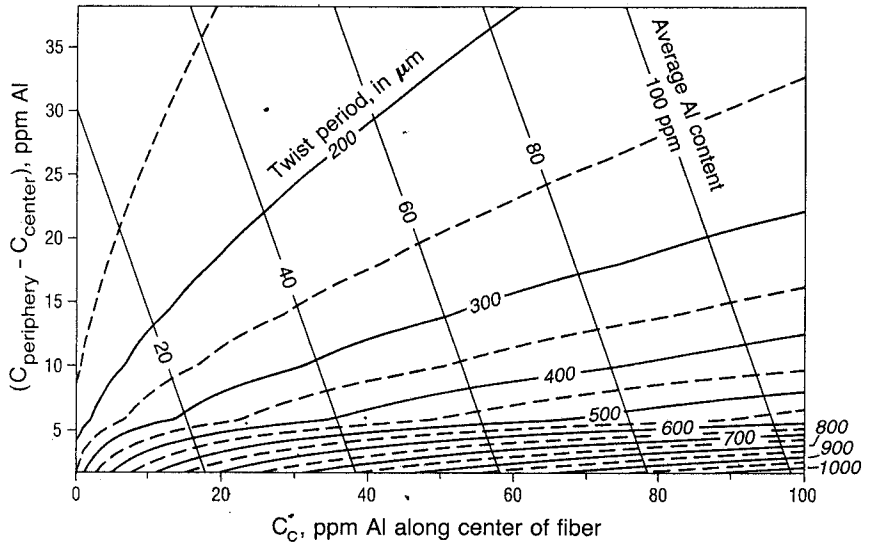

Fig. 3. Contours of twist period (solid contours are labelled in mμ; dashed ones are unlabellled) versus $(c_p - c_c)$ and c_c, calculated from eq 7 for a fiber of radius = 1 mμ. Also shown are contours for the average Al content in ppm's of a twisted fiber. During crystallization of agate layers and because of the dynamics illustrated in figure 1, a point representing the system moves repeatedly up and down on the left side of this diagram (with fibers becoming more and less twisted). Simultaneously, because of the spontaneous oscillations in the morphological instability of the growth front (Wang and Merino, 1995, fig. 7), the fibers become thin toward the top and thick toward the bottom of this diagram. This implies that very thin, tightly twisted fibers contain more Al than do less-thin, untwisted fibers. These predicted associated oscillating properties are just as observed in agates.

Merino (1990, figs. 2,3). Data acquisition was carried out with the program CHOIX, written by Claude Merlet of the University of Montpellier, designed for trace-element determination (Merlet and Bodinier, 1990). For a desired degree of confidence, the program calculates for each element the optimum counting time. Operating conditions were 60 nA of sample current and 20 kV. For the long 4.6 min counting time the beam size had to be 8 μm wide to avoid burning through the sample. The program calculates the relative error interval in percent for each analysis. The error yields the uncertainty (= 2σ = 0.5 × error percent × analytical value).

The Al contents are given in figure 4 as a cumulative frequency plot and are grouped into those for untwisted-fiber bands and those for twisted-fiber bands. Al contents of the five untwisted-fiber bands analyzed (thick line) range from 7 to 62 ppm (± 26) with weighted average about 32 ppm. Most of these for the five intervening twisted-fiber bands (thin line) range from 33 to 210 with weighted average about 62 ppm (± 26). K contents (not given here) cluster in the range 60 to 80 ppm for

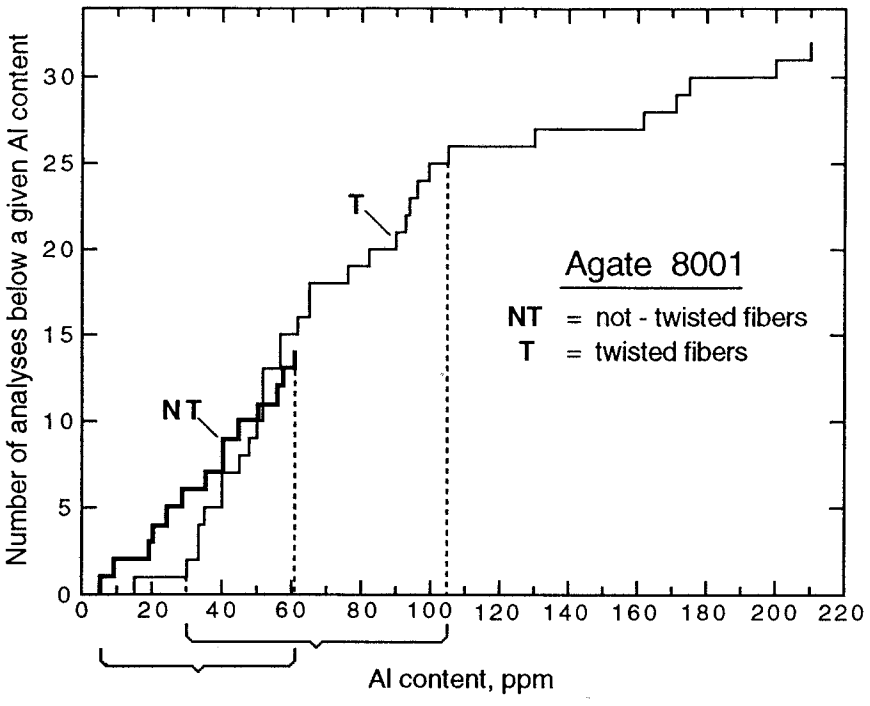

Fig. 4. Electron probe microanalyses for Al in agate 8001, Rio Grande do Sul, Brazil, given as the number of analyses falling below any given Al content, separately for twisted-fiber and untwisted-fiber chalcedony layers. Most of the analyses on twisted-fiber layers fall between 30 and 105 ppm Al, and all the analyses on untwisted-fiber layers fall below 60 ppm Al. The latter layers contain less Al than the former, as predicted by the self-organizational model (Wang and Merino, 1990, 1995).

the twisted-fiber bands (except for some zero ppm values) and 40 to 60 ppm for the untwisted-fiber bands. Na, Fe, and Ti contents are very uncertain (because they are at or below the level of detection) and are not reported here.

Because the electron beam was 8 μm wide and because the twisted quartz fibers are $\leq$ 1 μm, the analyses in figure 4 are really averages over several fibers. Spatial resolution is too coarse to test directly our prediction that $c_p > c_c$ for any one twisted fiber. A direct test of the twisting geometry embodied in eq (7) would require microanalyses with a spatial resolution of 0.1 μm or finer to be able to differenciate between the Al contents at the core and periphery of each twisted fiber.

The analyses of figure 4 (and also the ion-probe analyses given in the next section) are consistent with observations of cathode luminescence (Wang and Merino, 1990): pale blue luminescence (meaning very low Al—Henry and others, 1986) in the untwisted-fiber bands and no lumi-

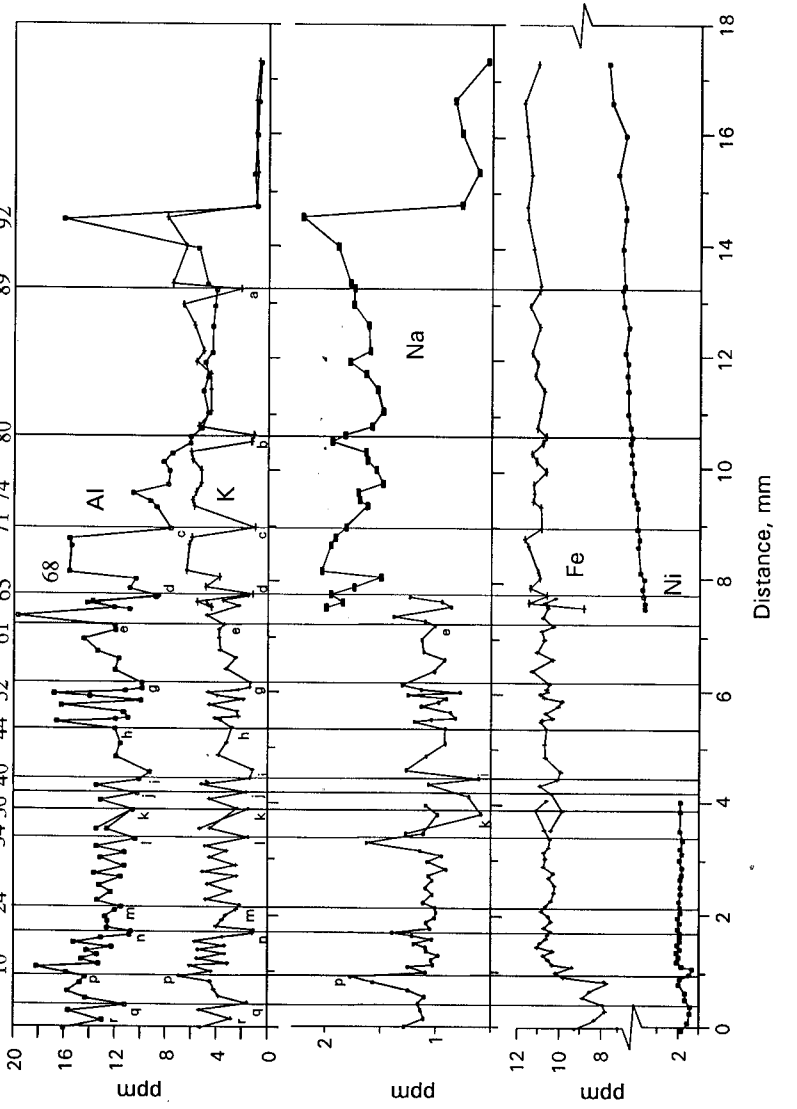

A.

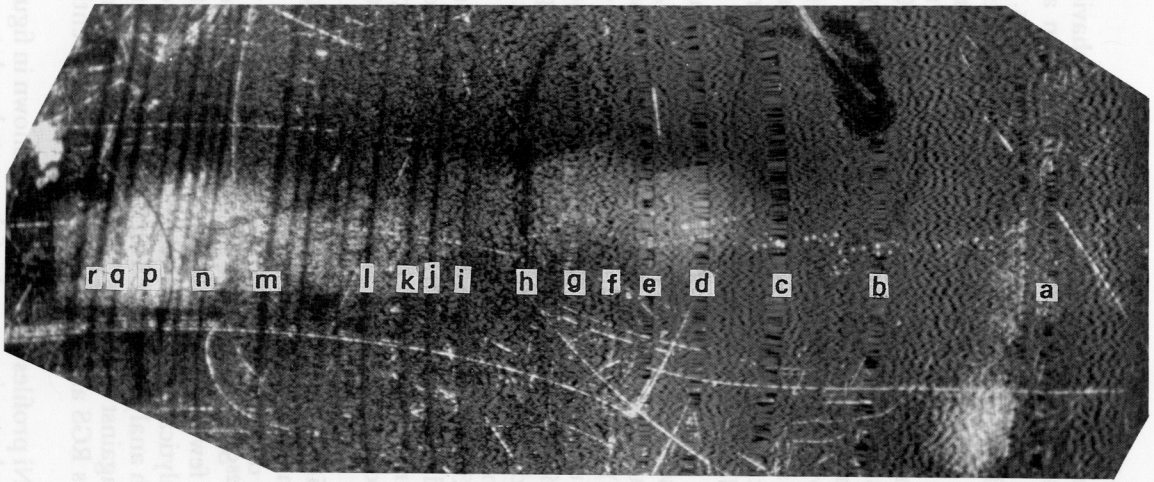

B.

Fig. 5. Ion-probe microanalyses shown in A for Al, K, Na, Ni, and Fe along a 17-mm profile of agate 8808 from the Paraná flood basalt, Rio Grande do Sul, Brazil. Analyses were obtained at spots 8 mμ wide, visible in the low-power photomicrograph shown in B. Along the top of A are a few analysis numbers plus the (dashed) boundaries between regions I (analyses 1-65), II (66-92), and III (93-110) for cross reference with figures 6 and 7. Analyses are numbered in sequence starting at left. Center of the agate is to the right. The agate portion corresponding to the composition profiles is also shown, under crossed polarizers and very low power. Each region has a distinctive quartz texture. Layers *a* to *e* of region II (consisting of stubby, untwisted fibers) display minima in Al, Fe, and K. The intervening bands, made of finer twisted fibers, are high in Al, Fe, and K. Band *f* was missed by the analytical points. The oscillation in K, Fe, and Al and their mutual correlation throughout regions I and II and their low (or high) values for untwisted (or twisted) fibers, all confirm the crystallization model described earlier (Wang and Merino, 1990, 1995). Region III corresponds to the drusy centimeter-sized length-slow quartz. See figures 6 to 8 and discussion on crystal chemistry in text.

nescence (meaning higher Al) in the twisted-fiber bands. (But note that Ramseyer and Mullis (1990) and Perny and others (1992) attributed luminescence to *high* Al contents. See Discussion of Twisting Mechanism.

ION-PROBE MICROANALYSES

In order to determine more accurately the contents and behavior of trace-elements, ion-probe analyses were made at 110 points on agate 8808, from Rio Grande do Sul. The points are in several traverses. The ion probe used was a modified Cameca IMS 3f at the Centre de Recherches Pétrologiques et Géochimiques, Nancy. A negative primary oxygen beam with intensity = 1.5−2 nA was focused to give a spot 8 to 10 μm wide. The positive secondary beam was energy-filtered at 80 ± 10 eV, and the mass resolution was set to 800. The secondary beam intensity was measured on the electron multiplier used in the counting mode.

Initial mass spectra covering the first 40 elements of the periodic table were carried out to see which trace elements are significant in sample 8808. Lithium is not present, Mg is present in amounts 2.5 orders of magnitude lower than Na, and Ca in amounts one order lower than Na. Hydrogen is low, and it is not given here because it can occur as water, OH^-, or hydrogen (which would be difficult to differentiate), and because instrumental moisture can add a significant background amount (which was not monitored). Potassium, Al, Fe, Mn, Ni, and Na were detected in significant amounts and were then systematically measured across the agate sample. Measurements were made by peak jumping. Two isotopes each of Si and Ni were measured independently to check for internal consistency, which was excellent. The analysis at each spot lasted 25 min, divided in 3 "blocs" of 9 cycles each. At each spot the sample surface was cleaned by sputtering the sample for 3 min before analyses. The energy filtering was achieved by centering the energy slit position with a nominal secondary high voltage at 4500 V, closing it to a range of 20 eV, and after adding a −80 V offset to the sample high voltage. The sample charging effects were corrected by measuring the energy distribution of ^{30}Si in each block. The intensity measured for each peak was normalized to ^{28}Si during the analysis. Typical count rates were 10^5 cps (counts per sec) on ^{28}Si and a few tens of cps for the other peaks, with the exception of only a few cps for ^{55}Mn. With a counting time of 108 sec on each ratio, the 2σ analytical errors ranged between 2 to 10 percent. The ratios obtained for each analysis were converted into concentrations in ppm by normalization against the ratios measured on two samples (fragments of agate samples RGS and 9045) analyzed independently by ICP.

The Na, K, Al, Fe, and Ni profiles (but not Mn) are shown in figure 5, along with a crossed-polars photomicrograph of the agate bands to which they belong. Clearly, K, Al, Fe, and Na contents oscillate and (mostly) oscillate together. From the outside towards the agate center Al decreases slightly, and total iron increases slightly. At the start of the coarse drusy

quartz (about 15 mm) Al, K, and Na decrease suddenly to less than 1 ppm each; Fe and Ni do not decrease.

DISCUSSION OF TRACE-ELEMENT COMPOSITION OF AGATE QUARTZ

The trace-element profiles of figure 5 directly confirm the oscillatory nature of agate crystallization. Minima in K, Al, and Fe, labelled *a* to *e* in figure 5, exactly correspond to the thin Group II layers consisting of untwisted and stubby quartz fibers, as predicted by the crystallization model (Wang and Merino, 1995). Minima *g* to *r* also correspond exactly to thin layers (those in Group I), but these can be identified petrographically only as brownish ribbons, with fiber twisting and fiber size remaining practically unchanged.

The analyses also point to significant crystal chemical relations and reactions in the agate quartz. The plot of ions believed to be substitutional (Al) versus ions believed to be interstitial (K+Na+2Fe+2Ni) is shown in figure 6; Fe and Ni, thought bivalent, are multiplied by 2. On figure 6 the analyses fall into three groups, each of which turns out to correspond to a specific region of the agate with a different quartz texture. Group I (analyses 1-65) corresponds to the outermost region, very finely banded and very finely fibrous (containing minima *g* to *r* in fig. 5A, B); alternative bands are pale brown under plane-polarized light. Group I analyses fall roughly on the unit-slope line passing through the origin, suggesting that Al substitutes for Si while all other cations occupy interstitial sites in the quartz structure and balance the Al (Smith and Steele, 1984). Potassium by itself also shows a linear correlation (not shown) with Al. Fe increases slightly while Al decreases slightly (fig. 5). Within Groups I and II many consecutive analyses go back and forth approximately along the 1:1 direction while simultaneously moving toward the southeast; this trend is schematically shown in the inset of figure 7 and can be seen in particular for analyses 1 to 5, 11 to 44, and 50 to 58.

Group II (analyses 66-92) corresponds to the banded region (containing minima *a* to *e* in fig. 5) where twisted-fiber and untwisted-fiber bands clearly alernate, both being easily distinguishable by their characteristic extinction patterns. Obviously, Group II analyses fall well below the 1:1 line. The large shift from Group I to II takes place suddenly between points 65 and 66 and is unaccompanied by changes in texture. We suspect this shift results from significant oxidation of ferrous to ferric iron, with total iron remaining approximately constant. The ferric iron would have to be added to the ordinates of figure 6 (since Fe^{3+} would be also substituting for Si), and the amount plotted on the abscissa would decrease (since only the ferrous iron would be interstitial). Group II analyses would then move toward better coincidence with the 1:1 line of figure 6. As the agate grows, the oxidation of Fe^{2+} to Fe^{3+} by water should take place to an increasing extent according to

$$Fe^{2+} + H_2O = Fe^{3+} + 0.5H_2 + OH^-, \quad (8)$$

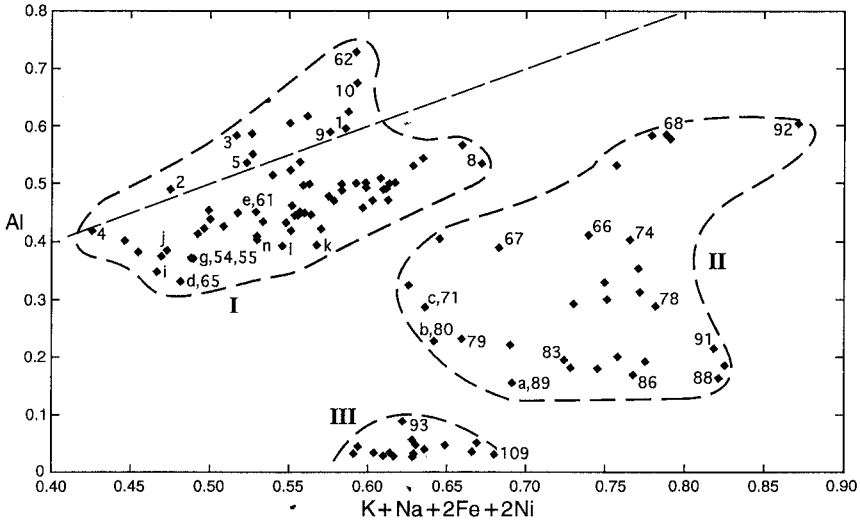

Fig. 6. Moles of Al versus (K+Na+2Fe+2Ni) moles for all ion-probe analyses shown in figure 5. A few analysis numbers and letter labels for minima from figure 5 are shown here for reference, and all are given in figure 7. Fe and Ni are supposed bivalent, at least in early stages of the agate growth. Groups I, II, and III correspond (see fig. 5, top) to the outer banded region of the agate, the inner banded region, and the coarse drusy region lining the central void, respectively. Group III includes ten analyses not shown in figure 5. Because Al roughly equals (K+Na+2Fe+2Ni) for Group I analyses, Al is thought to substitute for Si and the others to be interstitial in the quartz structure (Smith and Steele, 1984). Increasing generation of Fe^{3+} by reaction (8) probably drives some ferric iron to substitute for Si, thus pushing Group II analyses below and to the right of the 1:1 line (because the ferric portion should now be plotted on the ordinates but is not). The sudden change in quartz habit at 14.5 mm (see footnote 2) from very fine length-fast fibers to centimeters-sized length-slow crystals eliminates Al, Na, and K from the quartz, leaving only Fe and Ni in Group III. Extensive substitution of ferric iron for Si in region III makes the late drusy quartz increasingly darker purple amethyst.

a reaction necessarily driven to the right by the increases in both Fe^{2+} and H_2O concentrations automatically produced in the residual medium by withdrawal of silica from it (withdrawal of the silica with which the quartz layers are made). Reaction 8 is comparable to similar reactions in Sato (1978) and Deer, Howie, and Zussman (1992, p. 252) for other contexts.

Group III (nos. 93 to 109) corresponds to the coarse, length-slow,[2] drusy quartz lining the central void. Only analyses 93 to 97 are shown on figure 5A; number 98 to 109 are closely similar to those shown. All are plotted in figure 6. The large drusy crystals of quartz no longer accept Al, Na, and K, obviously because, being centimeter sized, they cannot be appreciably distorted—see eq 7—thus making no room for these cations.

[2] The sudden and routine change in optical orientation of agate quartz from length-fast to length-slow probably results from the inevitable passage of the silica units from *c*-parallel polymerized chains to isolated tetrahedra, a passage brought about by increasing water content of the residual medium upon crystallization of layers.

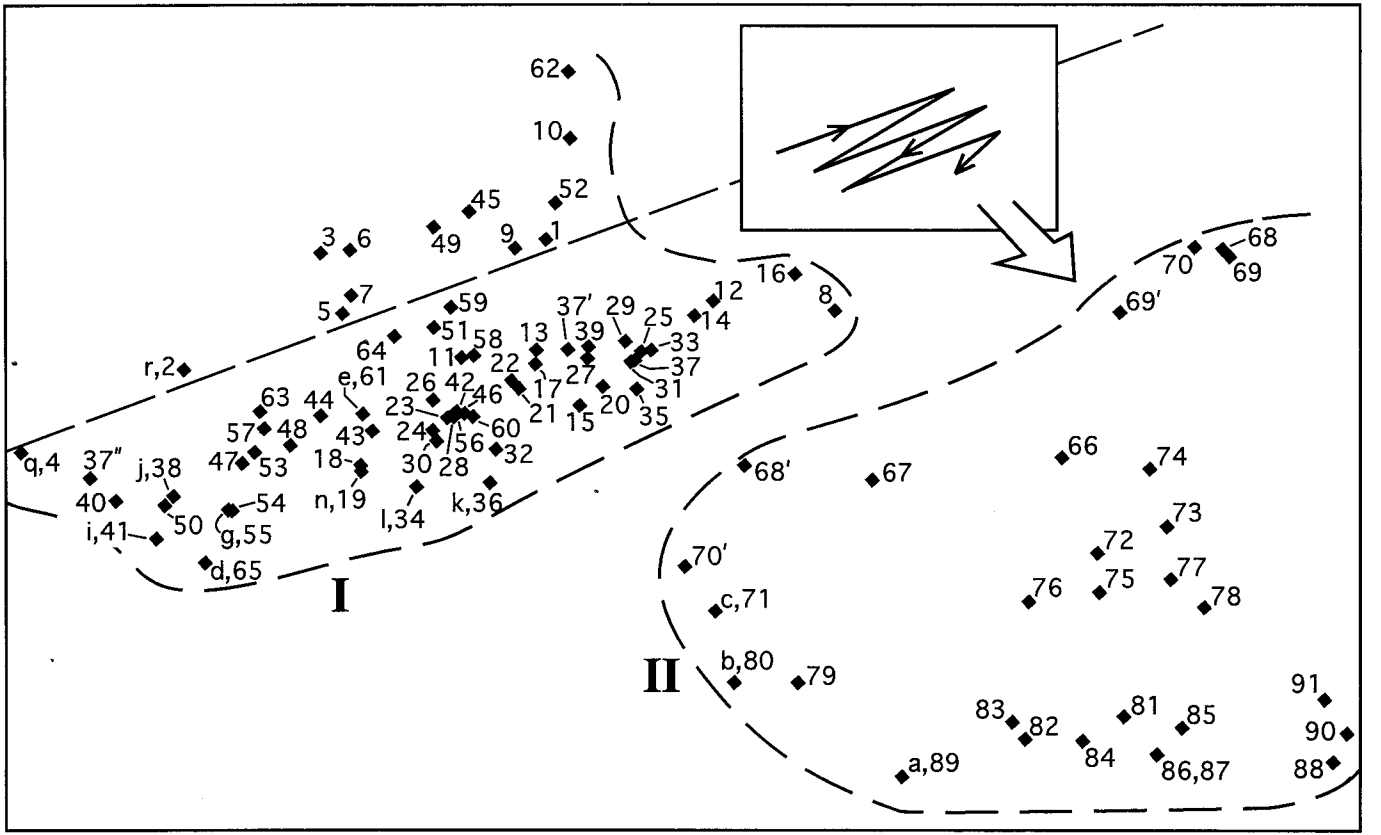

Fig. 7. Enlargement of figure 6 containing all analyses numbers in Groups I and II. It can be seen (but tie-lines are not included for clarity) that analyses 1 to 5, 11 to 44, and 50 to 58 go back and forth roughly along a unit-slope direction; these oscillations are as predicted in figures 6 and 7 of Wang and Merino (1995). Simultaneously many of the zig-zags gradually shift toward the southeast of the diagram, a shift probably reflecting oxidation of ferrous to ferric iron via reaction (8). The unit-slope oscillations and their gradual −1 slope shift (hollow arrow) are illustrated schematically in the inset.

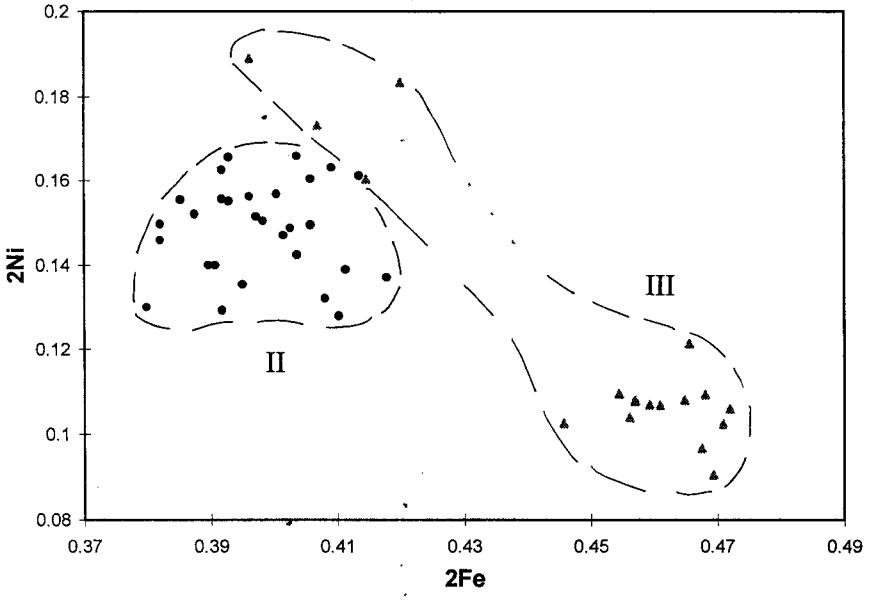

Fig. 8. Moles of Ni versus moles of total Fe for Groups II and III analyses, agate 8808. Group II corresponds to the agate portion containing bands *a* to *g* in figure 5. Group III analyses correspond to the late drusy centimeter-sized quartz and shift from northwest to southeast along a −1 slope line probably because of the increasing oxidation of ferrous to ferric iron, reaction (8).

The large crystals contain only Ni and Fe, which are plotted versus each other in figure 8. Again the analyses group themselves according to quartz texture: Group II forms a cluster centered at 0.2 and 0.08 for total Fe and total Ni, respectively. Group III analyses on the drusy quartz group themselves into two small clusters, both of them placed on a line of slope = −1. This distribution is also consistent with the increasing oxidation of ferrous to ferric (reaction 8), because analyses 98 to 110, the last ones, plot farther to the "southeast" along that line than analyses 93 to 97. Presumably, the increasing concentration of Fe^{3+} in the residual medium, coupled with depletion of Al^{3+} through incorporation in the quartz in the early stages of agate growth, brings about increasing substitution of Fe^{3+} for Si^{4+} in the latest quartz, which should therefore be purple (Cohen and Hassan, 1974; Cohen, 1985) and *increasingly* dark purple toward the agate's center. This is in fact seen in countless agates from Rio Grande do Sul. Fe^{3+} produced by reaction (8) can become so predominant over Fe^{2+} toward the end of the process as to drive co-growth of goethite needles included in the latest, drusy quartz; we have identified these needles, optically and by X-ray diffraction, in many samples. In addition, the alkalinity produced by eq (8) should promote zeolite growth (Hay, 1966; Bowers, Jackson, and Helgeson, 1984), as

observed in many agates. Prior to the discovery in the 50's of sedimentary zeolites, the only zeolites known were in fact those associated with agates.

Nickel not incorporated by the agate quartz (fig. 5) remains in the residual medium in the center of the agate, a medium that toward the end of the process inevitably becomes an aqueous solution of trace elements. Upon eventual flashing of this solution out of the microporous agate, the aqueous solution alters a thin film of surrounding basalt to layer silicates including the nickel-bearing gardnierite, which we have identified in two agates by xrd and by its distinctive dark green color.

In conclusion: trace elements in agate 8808 are well correlated with the changing quartz texture. Ion-probe analyses shown in figure 5A directly confirm the oscillations predicted by the crystallization model. On figure 6, Al analyses in Group I are roughly balanced by the sum of all others (Na, K, Ni, Fe) suggesting that Al substitutes for Si in quartz and the others are interstitial. The balance takes place even for sequential analyses, which can be seen on figure 7 to oscillate along a unit-slope line. The shift of these oscillations toward the "southeast" on figures 6 and 7 suggests that the amount plotted on abscissae is too large and that on ordinates too small; this in turn suggests that Fe^{2+} is becoming oxidized to Fe^{3+} (eq 8), which would then warrant transferring the Fe^{3+} (now probably substitutional) to ordinates, which would displace Group II analyses toward better agreement with the 1:1 line. Finally, operation of the oxidation (eq 8) is independently deduced from the general dynamics of close-system agate crystallization and supported by evidence for its products and consequences (final amethyst, final goethite, zeolite-agate association).

DISCUSSION OF THE PROPOSED TWISTING MECHANISM

We propose above that the twisting observed in agate chalcedony fibers is produced by differential substitution of trace elements (Al and Fe) for Si from the center to the periphery of fibers. Observed alternations in twist period are produced by alternations in the Al gradient in the medium through which the fibers grow. Here we discuss the geometric predictions in light of the trace-element analyses, crystal chemistry, and observed twist periods. The concept of twisting through solid solution hinges on agate quartz fibers's growing by accretion of conical sleeves (fig. 1), an experimental feature clearly observable (for another material) in figure 12 of Langer (1980).

Note that the numerator on the right of eq (7) is only slightly greater than 1 event for large Al contents in quartz, say 1000 ppm or more. Thus, the key factors detemining the twist period ℓ are the fiber radius and the difference in cube roots of Al contents at the periphery and center of the fiber. So, for the twist period of a fiber of a given radius to be short (that is, for tight twisting) the difference in the denominator of eq (7) must be relatively large. Note also that (because the $c^{1/3}$ function increases very steeply very near the origin of concentrations but very slowly for concen-

trations > 200 or 250 ppm) such large $c_p^{1/3} - c_c^{1/3}$ values needed for short twist periods, can be reached only for *low* average contents; large averages would require unreasonably large Al contents at the periphery of a fiber. But although our ion-probe trace-element analyses (fig. 5) are averages for whole fibers (which is why we have added contours for average Al content on fig. 3), one can still guess from the analyses that each twisted fiber's periphery and center do differ in trace-element composition, in the following way.

Because in agates the twist period jumps greatly from layer to layer (say, from 100 or 200 μm to 10^4 or 10^5 μm or more— Frondel, 1978), and because according to the proposed twisting hypothesis (with consequences displayed in fig. 3) the twisting period of thin fibers is far more sensitive to gradient changes when the average content is small than when it is large, we may infer that agates with drastic alternations in twist period from layer to layer should have modest trace-element average contents *and* modest $c_p - c_c$ values. The trace-element contents we have measured (fig. 5) are in fact low, which can be taken as partial confirmation of that inference. (For high average concentrations of trace metals, such as those reported by Graetsch, Flörke, and Miehe (1987), drastic changes of twisting period could only be caused by drastic differences in fiber thickness, not by changes in radial trace-element gradient, see eq 7, since twisting is no longer sensitive to it.)

It can be verified that a measured Al content of, say, 15 ppm (see fig. 5) together with, say, c_p = 20 ppm and c_c = 10 ppm (or with c_p = 16 ppm and c_c = 14 ppm) and with a fiber thickness on the order of 1 μm, when inserted into eq 7, yield twist periods precisely within the ranges observed in tightly-twisted fibers. Of course, if $c_p \rightarrow c_c$ within minute fractions of 1 ppm, then the twist period $\ell \rightarrow \infty$, as observed in untwisted fibers (with periods of 10^5 μm or more). In other words, eq 7 correctly connects observed or plausible values of twist period, fiber radius, and Al content, in both twisted and untwisted fibers.

The strengths of the proposed idea for fiber twisting by substitutional solid solution are: (1) the twisting is directly linked to the geochemical dynamics of agate growth, which is why the twist period itself alternates (in the model) from layer to layer, as observed; (2) it accounts not only for the twisting of single fibers but for the production of whole *textures* of twisted fibers, in which all the fibers are similarly oriented; (3) it accounts for the correct size of the twist period; (4) it accounts quantitatively for the observed close relationship among twisting, trace-element content, and fiber size; (5) it separates the genesis of the fibrosity from the genesis of the twisting (and both from the cause of the optical orientation of the fibers—see footnotes 1 and 2); and (6) it gives rise naturally to the microstructural defects observed by Graetsch, Flörke, and Miehe (1987), Heaney (1993), and Cady and others (1993): the defects would result simply from annealing of the twisting.

The twisting of fibers should destroy some symmetry relative to untwisted quartz, via ordering of the aluminum ions (brought about by

strain—Wang and Merino, 1990) and/or because of the twisting itself, which takes place about [11$\bar{2}$0] or more rarely [1$\bar{1}$00] (Frondel, 1978; Michel-Lévy and Munier-Chalmas, 1892). The moganite reported in agates by Graetsch, Flörke, and Miehe (1987) and Heany and Post (1992) may be just this lower-symmetry twisted quartz or its annealed product (since lamellar Brazil twins, of which moganite consists, and planar defects are also reported). Some weaknesses in accounting for the observed agate textures through the screw-dislocation fiber twisting-mechanism envisioned by Frondel (1978) and Heaney (1993) were discussed by Wang and Merino (1990, p. 1636).

Twisted chalcedony fibers (though not arranged in layers of alternating twist period as in agates) also occur in some chert concretions in sedimentary rocks (Milliken, 1979, and our own observations). Our crystal-growth model for fibrosity through morphologically unstable crystallization fronts (Wang and Merino, 1995) and for twisting of fine fibers also may apply to the sedimentary concretion occurrences cited. This will be discussed elsewhere.

CONCLUSIONS

The fibrous texture of agate quartz is produced by morphologically unstable cyrstallization fronts; each fiber grows by adding conical sleeves, which pierce through the concentration profiles of trace elements decreasing away from the front (Wang and Merino, 1995). The base of each sleeve incorporates more Al^{3+} (and/or Fe^{3+}) than its tip. As a result, the quartz fiber contains more Al^{3+} (or Fe^{3+}) along its periphery than along its center. Because Al^{3+} (or Fe^{3+}) ions are larger than Si, the fiber must grow twisted to accommodate the additional peripheric Al^{3+} (or Fe^{3+}) content and to maintain structural continuity. A geometric calculation yields the dependence of twisting period on fiber's radius, average Al content, and Al-content difference between a fiber's periphery and center. The genetic model (Wang and Merino, 1995) predicts the alternation of layers consisting of fine, untwisted, and low-trace-element-content fibers with layers consisting of finer, twisted, and high-trace-element content fibers. The prediction is confirmed by electron microprobe and ion microprobe analyses. The difference in Al (and/or Fe^{3+}) content between a fiber's periphery and center cannot be measured directly with the ion-probe (because the fibers are too thin), but is estimated to be 5 to 15 ppm. Al^{3+} and Fe^{3+} both substitute for Si^{4+}, but to different degrees in different portions of the agate. In the two agates analyzed, K is the main monovalent ion to balance the charge deficit produced by (Al + Fe^{3+})-for-Si substitution, but Na, Ni, and Fe^{2+} also help balancing that deficit. Ferric iron, not present in the initial medium, is produced by oxidation of ferrous iron by H^+ in H_2O. The oxidation is driven by an inevitable inward increase in chemical potentials of Fe^{2+} and H_2O in the residual medium in the agate's center, an increase produced by the very growth of chalcedony under closed-system. The length-fast, fibrous, twisted/untwisted, and banded texture of the chalcedony layers results directly

from the dynamics of silica and trace-element behavior in the initial medium. But toward the end of the process, when the residual medium must become more aqueous, silica building blocks in the medium switch from *c*-parallel polymeric chains to isolated tetrahedra. Now the quartz produced becomes length-slow. In addition, if at this point the crystallization front becomes morphologically stable (which is usually the case in agates), the crystals become non-fibrous and large. Being large, they can no longer grow twisted (eq 7), thus must stop incorporating Al, Na, and K, as observed. If the front continued to be morphologically unstable then growth of length-slow fine fibers would ensue, as occasionally observed.

ACKNOWLEDGMENTS

We are very grateful to our friends Yutian Wang, on leave in Bloomington from Changchun University of Earth Sciences, Fabrice Colin, Bruno Hamelin, and Daniel Nahon of the University of Aix-Marseille III, and Sam Savin of Case Western Reserve University, for help, discussion, and additional electron microprobe analyses not reported here; to Milton Formoso and colleagues of the Federal University of Rio Grande do Sul at Porto Alegre for taking us on an enlightening fieldtrip to agate quarries near Salto de Jacuí; to Rejane M. Scopel also of Porto Alegre for sending us unpublished photomicrographs from her 1990 thesis; to Claude Merlet of the Service Commun de Microsonde at the University of Montpellier II for invaluable analytical skill and guidance; to Lorie Canada, Jim Tolen, Kim Sowder, and Barbara Hill of Indiana University for expert assistance; to Qijiang Ren of Nanjing University, Brian Jacskon of the Royal Museum of Scotland at Edinburgh, and Roy Young of Nature's Own (Nederland, Colorado), for spontaneously giving us Chinese, Scottish, and Brazilian agates, respectively; to P. Heaney (Princeton) and P. Van Cappellen (Georgia Tech) for careful critical reviews that have helped us improve the manuscript; to the Exchange Program between Nanjing and Indiana Universities for crucial support to Yifeng Wang with a fellowship, 1988–1990; to the Laboratory for Environmental Geosciences and its director, Daniel Nahon (University of Aix-Marseille III), for generous logistic, financial, travel, and analytical support to us while on sabbatical there; and to the U.S. National Science Foundation for support of this research through grants EAR 90-03633 and 91-04198 to Merino. This article is contribution number 1101 of the Centre de Recherches Pétrologiques et Géochimiques.

REFERENCES

Bowers, T. S., Jackson, K. J., and Helgeson, H. C., 1984, Equilibrium Activity Diagrams: Berlin, Springer-Verlag, 397 p.

Cady, S. L. Wenk, H.-R., Kilaas, R., and Barber, D. J., 1993, Enantiomorphism and planar defects in length-fast chalcedony, *in* Boland, J. N., and Fitz Gerald, J. D., editors, Defects and Processes in the Solid State, Geoscience Applications. The McLaren Volume: Amsterdam and New York, Elsevier, p. 383–400,

Cohen, A. J., 1985, Amethyst color in quartz, the result of radiation protection involving iron: American Mineralogist, v. 70, p. 1180–1185.
Cohen, A. J. and Hassan, F., 1974, Ferrous and ferric ions in synthetic α-quartz and natural amethyst: American Mineralogist, v. 59, p. 719–728.
Deer,W. A., Howie, R. A., and Zussman, J., 1992, An Introduction to the Rock-Forming Minerals: Essex and New York, Longman and Wiley, 696 p.
Folk, R. L. and Pittman, J. S., 1971, Length-slow chalcedony: A new testament for vanished evaporties: Journal of Sedimentary Petrology, v. 41, p. 1045–1058.
Frondel, C., 1978, Character of quartz fibers: American Mineralogist, v. 63, p. 17–27.
Geisinger, K. L., Gibbs, G. V., and Navrotsky, A., 1985, A molecular orbital study of bond length and angle variations in framework structures: Physics and Chemistry of Minerals, v. 11, p. 266–283.
Gonthier, E., Skrok, J., Apter, M., and Fröhlich, Fl., 1988, L'Univers des Agates: Revue de Gemmologie (special issue for an exhibit at the Museum National d'Histoire Naturelle, Paris), p. 12.
Graetsch, H., Flörke, O. W., and Miehe, G., 1987, Structural defects in microcrystalline silica: Physics and Chemistry of Minerals, v. 14, p. 249–257.
Hay, R. L., 1966, Zeolites and zeolitic reactions in sedimentary rocks: Geological Society of America Special Paper, v. 85, p. 130.
Heaney, P. J., 1993, A proposed mechanism for the growth of chalcedony: Contributions to Mineralogy and Petrology, v. 115, p. 66–74.
Heaney, P. J., and Post, J. E., 1992, The widespread distribution of a novel silica polymorph in microcrystalline quartz varieties: Science, v. 255, p. 441–443.
Henry, D. J., Toney, J. B., Suchecki, R. K., and Bloch, S., 1986, Development of quartz overgrowths and pressure solution in quartz sandstones: Evidence from cathodoluminescence/back-scattered electron imaging and trace-element analysis on the electron microprobe: Geological Society of America Abstracts with Programs, v. 18, p. 635.
Keith, H. D. and Padden, F. H., Jr., 1961, Note on the origin of twisting orientation in fibrillar crystals: Journal of Polymer Science, v. 51 (156), p. S4–S7.
Langer, J. S., 1980, Instabilities and pattern formation: Reviews of Modern Physics, v. 52, p. 1–28.
Macpherson, H. G., 1989, Agates: Edinburgh and London, National Museums of Scotland and the British Museum, p. 72.
Merino, E., 1984, Survey of geochemical self-patterning phenomena, *in* Nicolis, G., and Baras, F., editors, Chemical Instabilities: NATO Advanced Science Series C, v. 120, p. 305–328.
Merino, E., Harvey, C., and Murray, H. H., 1989, Aqueous-chemical control of the tetrahedral-aluminum content of quartz, halloysite, and other low-temperature silicates: Clays and Clay Minerals, v. 37, p. 135–142.
Merino, E., Wang, Yifeng, and Deloule, E., 1994, Genesis of banded, fibrous, and twisted quartz by 'catalysis,' unstable crystallization fronts, and substitution: self-organization in agates: Mineralogical Magazine, v. 58A, p. 597–598.
Merlet, C. and Bodinier, J. L., 1990, Electron microprobe determination of minor and trace transition elements in silicate minerals: A method and its application to mineral zoning in the peridotite nodule PHN1611: Chemical Geology, v. 83, p. 55–69.
Michel-Lévy, A., and Munier-Chalmas, E., 1892, Mémoire sur diverses formes affectées par le réseau élémentaire du quartz: Bulletin de la Société Française de Minéralogie, v. 15, p. 161–190.
Milliken, K. L., 1979, The silicified evaporite syndrome—Two aspecsts of silicification history of former evaporite nodules from southern Kentucky and northern Tennessee: Journal of Sedimentary Petrology, v. 49, p. 245–256.
Nicolis, G. and Prigogine, I., 1977, Self-Organization in Non-Equilibrium Systems: New York, Wiley. p. 491.
———— 1989, Exploring Complexity: An Introduction: New York, W.H. Freeman, p. 313.
Perny, B., Eberhardt, P., Ramseyer, K., and Pankrath, R., 1992, Microdistribution of Al, Li and Na in α quartz: Possible causes and correlation with short-lived cathodoluminescence: American Mineralogist, v. 77, p. 534–544.
Ramseyer, K., and Mullis, J., 1990, Factors influencing short-lived cathodoluminescence of α-quartz: American Mineralogist, v. 75, p. 791–800.
Sato, M., 1978, Oxygen fugacity of basaltic magmas and the role of gas-forming elements: Geophysical Research Letters, v. 5, p. 447–449.

Smith, J. V., and Steele, I. M., 1984, Chemical substitution in silica polymorphs: Neue Jahrbuch Mineralogie, Monahefte; v. H3, p. 137–144.
Wang, Yifeng, and Merino, E. 1990, Self-organizational origin of agates: Banding, fiber twisting, composition, and dynamic crystallization model: Geochimica et Cosmochimica Acta, v. 54, p. 1627–1638.
———— 1995, Origin of fibrosity and banding in agates from flood basalts: American Journal of Science, v. 295, p. 49–77.
Wedephol, K. H., 1970, Handbook of Geochemistry, v. II/2: Berlin, Heidelberg, New York, Springer-Verlagy.